

DNA-Patched Nanoparticles for the Self-Assembly of Colloidal Metamaterials

Le Liang,[#] Lintong Wu,[#] Peng Zheng,[#] Tao Ding, Krishanu Ray, and Ishan Barman^{*}



Cite This: *JACS Au* 2023, 3, 1176–1184



Read Online

ACCESS |

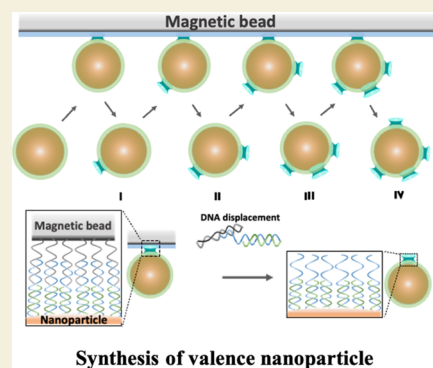
Metrics & More

Article Recommendations

Supporting Information

ABSTRACT: Colloidal metamaterials are highly desired artificial materials that recapitulate the structure of simple molecules. They exhibit exceptional functionalities conferred by the organization of and specific interaction among constituent elements. Harvesting such exquisite attributes for potential applications necessitates establishing precise control over their structural configuration with high precision. Yet, creating molecule-like small clusters of colloidal metamaterials remains profoundly challenging, as a lack of regioselectively encoded surface chemical heterogeneity prevents specific recognition interactions. Herein, we report a new strategy by harnessing magnetic-bead-assisted DNA cluster transferring to create discretely DNA cluster-patched nanoparticles for the self-assembly of colloidal metamaterials. This strategy affords broad generalizability and scalability for robustly patching DNA clusters on nanoparticles unconstrained by geometrical, dimensional, and compositional complexities commonly encountered in colloidal materials at the nano- and microscale. We directly judiciously patched nanoparticles into a wide variety of nanoassemblies and present a case study demonstrating the distinct metamaterial properties in enhancing the spontaneous emission of diamond nanoparticles. This newly invented strategy is readily implementable and extendable to construct a palette of structurally sophisticated and functionality-explicit architecture, paving the way for nanoscale manipulation of colloidal material functionalities with wide-ranging applications for biological sensing, optical engineering, and catalytic chemistry.

KEYWORDS: *self-assembly, valence nanoparticles, metamaterials, diamonds*



1. INTRODUCTION

Colloidal materials, as exemplified by metallic nanoparticles, solid-state quantum emitters, and polymeric nanoparticles, possess unique optical, magnetic, and electronic properties with a wide array of applications in biomedicine, optics, and catalytic reactions.^{1–8} While tunable by manipulating the size, shape, or surface chemistry at the single nanoparticle level, their achievable functionalities are typically limited by the finite behaviors intrinsic to a given nanoparticle.^{9–11} To enrich the properties of colloidal materials and extend their applicability, there is a growing demand for rational design and judicious assembly of nanoparticles bearing distinct functionalities.^{12–16} This is because structurally diverse and compositionally heterogeneous nanoassemblies, also called colloidal metamaterials, exhibit many coveted properties derived from the synergistic effects of the constituent nanoparticles, which are rarely or never seen at the single nanoparticle level.^{1,4,17,18} In particular, small clusters of colloidal metamaterials with a low coordination number that recapitulate the structure of simple molecules permit customizing and fine-tuning of the material attributes conferred by the organization of and the specific interaction among constituent nanoparticles.^{19–21} Harvesting such exquisite material attributes for potential applications, thus, necessitates establishing precise control over their

structural configuration with high fidelity.^{22–25} Yet, it remains profoundly challenging to fabricate molecule-like small clusters of colloidal metamaterials with desired architecture, as a lack of regioselectively encoded surface chemical heterogeneity prevents specific recognition and interactions among constituent nanoparticles, a prerequisite for programmable colloidal self-assembly.^{26–29}

Such challenges can be potentially addressed by the discrete surface encoding of colloidal nanoparticles with heterogeneous surface patches.^{30,31} The specific binding between mutually attractive surface patches would endow atom-like colloidal nanoparticles with valence-equivalent functionalities and therefore direct the self-assembly of surface-patched nanoparticles into higher-order structures in the same manner as the formation of molecular structures from atomic interactions.^{1,26} Despite the conceptual simplicity, it remains challenging to design patch materials that permit individual control over the

Received: January 22, 2023

Revised: March 10, 2023

Accepted: March 10, 2023

Published: March 29, 2023



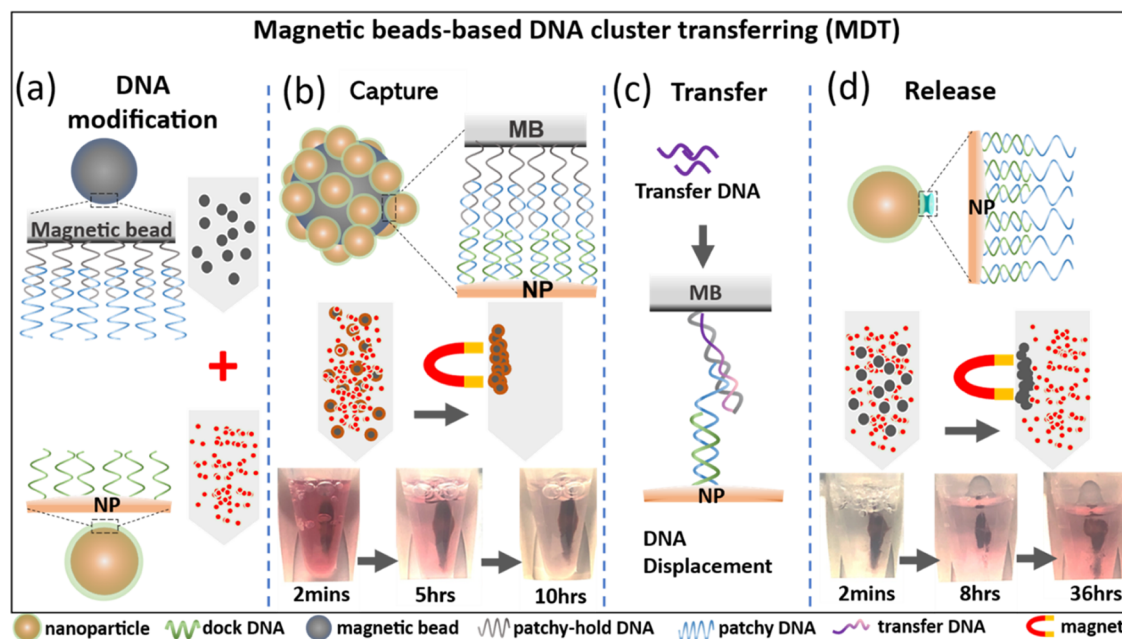


Figure 1. Principle of magnetic bead-based DNA cluster transferring. The nanoparticles are precoated with dock DNA (green). Magnetic beads are coated with patchy-hold DNA (gray), and a toehold domain is reserved on the patchy-hold DNA for transfer DNA (purple). The patchy-hold DNA can hybridize with the patchy DNA (blue). The patchy DNA consists of two domains: the anti-patchy-hold domain, which is complementary to the patchy-hold DNA, and the antidock domain, which can hybridize with the dock DNA. Schematics for (a) DNA modification, (b) capture process of gold nanoparticles by magnetic beads, (c) addition of transfer DNA to initiate DNA displacement, and (d) release of patched nanoparticles. Photographs in (b, d) show the dynamic capture and release processes of gold nanoparticles.

chemical and biochemical heterogeneity to realize directional and specific binding (i.e., orthogonality). Exacerbating the difficulty is a lack of robust discrete surface encoding strategies that are compatible with geometrically, dimensionally, and compositionally diversified colloidal nanoparticles.²⁹ While complementary reactive polymers serving as attractive surface patches have been recently demonstrated to allow the fabrication of colloidal metamaterials with well-defined structures, the achieved directional and specific binding through electrostatic repulsion and stoichiometric reactions limits the extent of their applicability.^{9,26} The resulting large interparticle gap from the polymer coating further compromises the collective interaction of the constituent nanoparticles, which is crucial to maximizing the performance of colloidal metamaterials such as for surface-enhanced Raman sensing.

An alternative but the far more promising strategy is to employ DNA clusters as surface patches to encode the desired orthogonality on colloidal nanoparticles, as synthetic DNA sequences can be arbitrarily customized and allow highly robust, specific, and reversible interactions. Recent advances have established proof-of-concept demonstrations of creating atom-like single-stranded DNA (ssDNA) sequence-encoded small gold nanoparticles (5–30 nm) for colloidal self-assembly.²⁸ A relevant strategy has also been proposed to transfer DNA patterns to small gold nanoparticles (~10 nm).^{31–33} The effectiveness of these approaches, however, is limited to addressing only small gold nanoparticles, as the surface-encoded ssDNA sequence proves less effective in the direct self-assembly of dimensionally diverse nanoparticles. Using DNA patches, which contain a cluster of ssDNA sequences, the interaction strength between complementary DNA patches can be significantly augmented and leveraged to drive the self-assembly of large nanoparticles, as has been

demonstrated in the fabrication of DNA origami templated colloidal metamaterials.^{19,21,34} In light of these advances, we hypothesize that devising DNA clusters instead of ssDNA sequences to discretely patch constituent nanoparticles can afford the highly desired orthogonality to break the homogeneous surface chemistry for programming colloidal metamaterials with high precision.

In this study, we propose a new strategy by harnessing magnetic bead-assisted DNA cluster transferring (MDT) to create discrete DNA patches on nanoparticles for the self-assembly of colloidal metamaterials. To address the limited applicability, lack of scalability, and geometrical and dimensional restrictions of previously reported approaches, we have established a generalizable and readily implementable protocol for transferring DNA clusters to colloidal nanoparticles unbound by their geometry, dimension, and composition. The use of magnetic beads to assist the transfer of DNA clusters and purification of patched nanoparticles precludes the need for centrifugation, which has often been a crucial yet detrimental step in extracting patched nanoparticles. The judiciously patched nanoparticles are further directed through spontaneous DNA hybridization to form a wide variety of nanoassemblies, with a use case demonstrating the exceptional metamaterial attributes of silver cubic dimers in simultaneously enhancing the fluorescence intensity and emission rate of nitrogen-vacancy (NV) centers in nanodiamonds.

2. RESULTS AND DISCUSSION

2.1. Magnetic Bead-Based DNA Cluster Transferring (MDT)

The proposed MDT strategy involves four steps: DNA modification, nanoparticle capture, DNA cluster transfer, and patched nanoparticle release, as schematically shown in Figure 1. Initially, gold nanoparticles are precoated with a dense layer

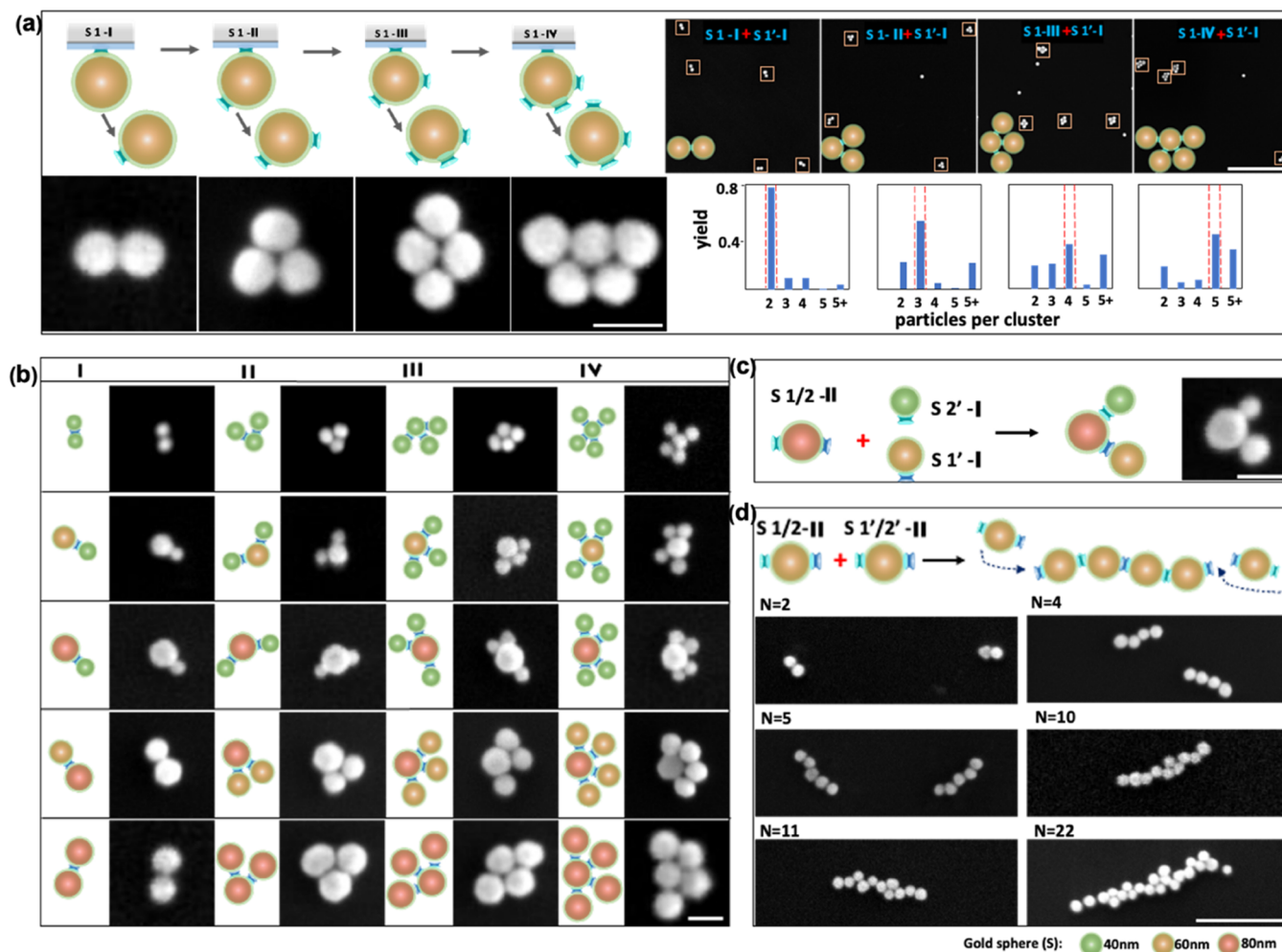


Figure 2. Design, demonstration, and SEM characterization of DNA self-assembled spherical nanoassemblies with multivalent colloidal nanoparticles. (a) Left: diagram of colloidal gold nanoassemblies with the same size of 60 nm but an increasing number of valence bonds. The patched colloidal nanoparticles are called monovalent (S1-I), divalent (S1-II), trivalent (S1-III), and tetravalent (S1-IV), where “1” represents the type-I DNA patch and “I, II, III, and IV” stand for the number of patches. The zoom-in SEM images of the synthesized nanoparticles; scale bar: 100 nm. Right: large SEM images along with estimated yields of the synthesized nanoparticles; scale bar: 1 μm . (b) Gold spherical nanoassemblies with different size combinations, as indicated. Scale bar: 100 nm. (c) Size-heterogeneous trimer nanoassembly. Scale bar: 100 nm. (d) Linear oligomer nanoassemblies (60 nm in diameter) with different lengths. Scale bar: 1 μm .

of dock DNA (green), while magnetic beads are functionalized with patchy-hold DNA (gray). A toehold domain is reserved on the patchy-hold DNA for subsequent DNA displacement. The patchy-hold DNA is further hybridized with the patchy DNA (blue). The patchy DNA consists of two domains, i.e., the anti-patchy-hold domain that is complementary to the patchy-hold DNA and the antidock domain that can hybridize with the dock DNA. Therefore, by mixing the above-mentioned DNA-modified gold nanoparticles with magnetic beads and through hybridization of the antidock domain of the patchy DNA with the dock DNA, gold nanoparticles are captured by the magnetic beads. In this reaction, a particle concentration ratio of 10,000:1 for gold nanoparticles to magnetic beads is used, which, combined with the steric hindrance of magnetic beads, eliminates the possibility of one gold nanoparticle captured by two or more magnetic beads. The dynamic capture process of gold nanoparticles by magnetic beads is manifested in the fading red color as seen for the liquid solution in the centrifuge tube in the presence of a magnet. Owing to the attractive force of the magnet, gold nanoparticle-bonded magnetic beads become gradually at-

tached to the magnet, leaving behind a small number of free gold nanoparticles in the solution.

To complete the DNA cluster transfer, the transfer DNA (purple) is introduced into the solution of purified magnetic beads coated with AuNPs. The transfer DNA is specifically designed to be complementary to the patchy-hold DNA. It can nucleate at the toehold domain of the patchy-hold DNA to initiate DNA strand migration. Hybridization of the transfer DNA with the patchy-hold DNA thus detaches the patchy DNA, leading to the release of gold nanoparticles from the magnetic beads. The dynamic release process is evidenced by the gradual recovery of the red color that is specific to the gold nanoparticles. At the completion of the release process, the patchy DNA is precisely transferred to the regioselective domain of the gold nanoparticles in contact with the magnetic beads.

It is noted that surface encoding with DNA patches endows colloidal nanoparticles with specific surface functionalities analogous to a valence bond.¹⁶ In this study, the number of DNA patches transferred is thus defined as the valence of the patched colloidal nanoparticles. For each MDT process, one

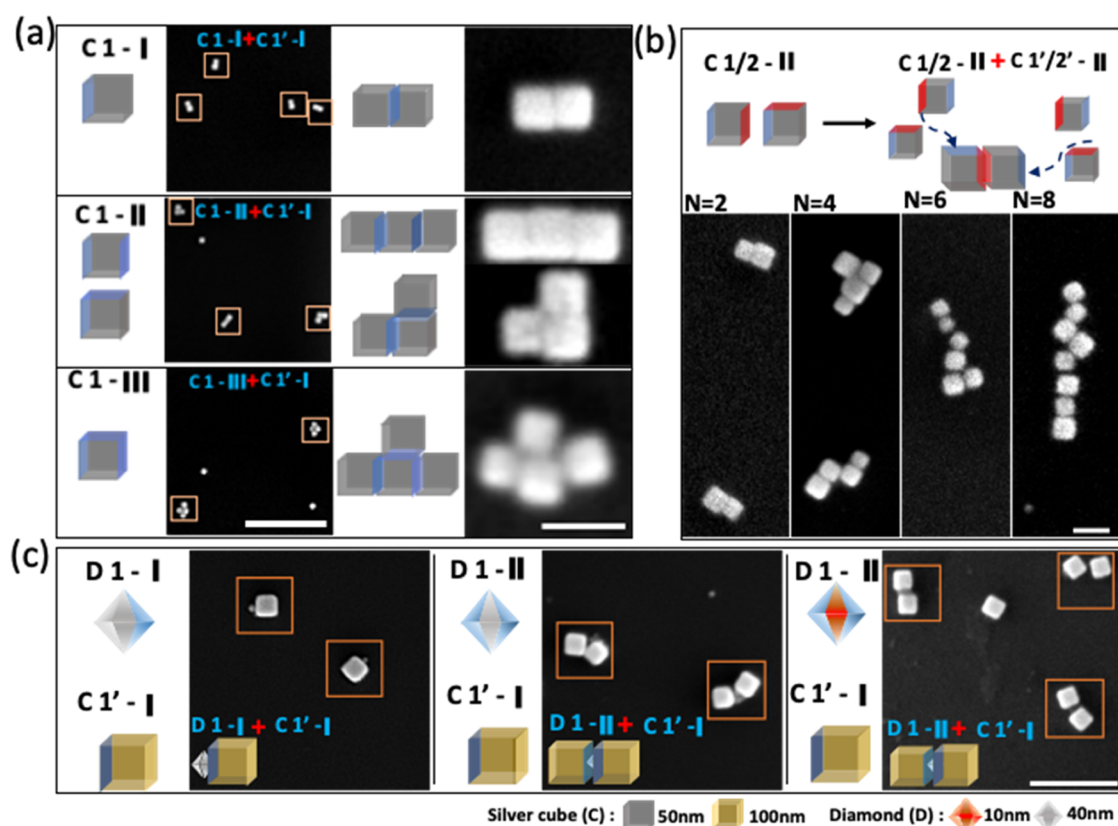


Figure 3. Expanded demonstration and SEM characterization of nonspherical nanoassemblies. (a) Colloidal silver cube nanoassemblies with the same size of 50 nm but an increasing number of valence bonds. Scale bar: 1 μm (left) and 100 nm (right). (b) Silver nanocube-based linear oligomer nanoassemblies with different lengths. Scale bar: 100 nm. (c) Compositionally heterogeneous nanoassemblies using silver nanocubes and geometrically irregular diamond nanoparticles. Scale bar: 500 nm.

valence is added to the colloidal nanoparticles. The MDT process can be repeated to add additional valences. The added valences can either be homogeneous with the same DNA sequences or heterogeneous with different ones. Owing to the programmability of the valences and DNA sequences, the homogeneity of the surface chemical environment commonly seen for colloidal nanoparticles can be broken by the regioselective MDT strategy with defined valences conferred. It can be reasoned that, through specific and directional DNA hybridization, patched colloidal nanoparticles can spontaneously form a variety of nanoassemblies in the same manner as a molecular reaction with stoichiometry control. As the MDT process is not predicated on the specific geometry, size, and composition of the colloidal nanoparticles and is centrifugation-free, the strategy can be generalized to patch arbitrary colloidal nanoparticles, which lends enormous flexibility to fabricate desired colloidal nanoarchitecture unbound by geometrical, dimensional, or compositional complexities. It is worth noting that DNA origami nanostructures and single DNA sequences allow specific and directional DNA hybridizations and have been leveraged for the self-assembly of various types of nanoassemblies.^{19–21} Nevertheless, the DNA patches and the MDT strategy presented in this study provide a complementary approach to realizing the self-assembly of metamolecules.

2.2. Constructing Spherical Nanoassemblies with Multivalent Colloidal Nanoparticles

The utility of the MDT strategy is first demonstrated by fabricating gold spherical nanoassemblies with increasing

complexity. To start with, a given valence of the DNA patch is added to the colloidal gold nanoparticles. Here, the patched colloidal nanoparticles are called (and represented by) monovalent (S1-I), bivalent (S1-II), trivalent (S1-III), tetravalent (S1-IV), etc., where “1” represents type-1 DNA patch and “I, II, III, and IV” stand for the number of patches, as shown in Figure 2a. The symbol for monovalent colloidal nanoparticles complementary to type-1 DNA patch is given by S1'-I. Likewise, the heterogeneous DNA patches (type-1 and type-2 DNA sequences) are represented by S1/2-II. The monovalent colloidal nanoparticles complementary to S1/2-II are given by S1'-I and S2'-I (Figure 2c), while the bivalent colloidal nanoparticles complementary to S1/2-II are represented by S1'/2'-II (Figure 2d).

Following the above-mentioned principle, core-satellite gold nanoassemblies with different levels of complexities are constructed (Figure 2a–c). This is achieved by first adding a given number of homogeneous multivalences to the core gold nanoparticles, making them monovalent (S1-I), bivalent (S1-II), trivalent (S1-III), and tetravalent (S1-IV), respectively. The satellite gold nanoparticles are made monovalent (S1'-I) with complementary sequences to the valences on the core nanoparticles. For the same size (60 nm in diameter) of patched core and satellite gold nanoparticles, four representative nanoassemblies with mono-, di-, tri-, and tetravalent bonding modes are formed following DNA hybridization, as confirmed by scanning electronic microscopy (SEM) imaging (Figure 2a). The yield for the formed dimer, trimer, tetramer, and pentamer is estimated to be 78, 52, 34, and 42%,

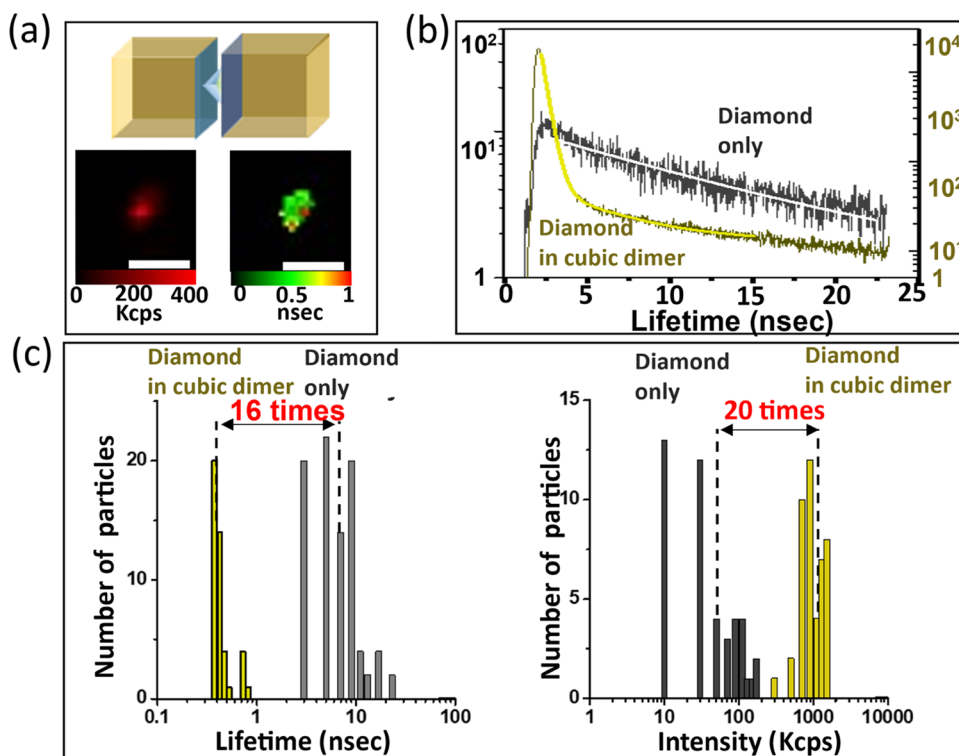


Figure 4. Silver cubic dimer-enhanced spontaneous emission of a diamond nanoparticle. (a) Schematic of the 100 nm silver cubic dimer with a 40 nm nanodiamond sandwiched in between and the corresponding fluorescence intensity and lifetime images. (b) Lifetime decay of the silver cubic dimer with a diamond nanoparticle sandwiched in between as compared to that of a bare diamond nanoparticle. (c) Statistical analysis of the average lifetime reduction and intensity enhancement as compared to that of a bare diamond nanoparticle. Scale bar 1 μ m.

respectively, based on a statistical analysis of the SEM images (Section S11 and Tables S2 and S3).

To demonstrate the nanoparticle size compatibility of the MDT strategy, homogeneous multivalent core and monovalent satellite gold nanoparticles with different diameters (40, 60, and 80 nm) are prepared. Through DNA hybridization, gold spherical nanoassemblies with different size combinations are obtained (Figure 2b). More SEM images of gold spherical nanoassemblies with different size combinations are provided in Figures S1–S5, with the yield summarized in Table S1.

The possibilities of the MDT strategy are further demonstrated by preparing heterogeneous multivalent nanoparticles. As shown in Figure 2c, a size-heterogeneous trimer nanoassembly (core: 80 nm; satellite: 60 and 40 nm) is created through DNA hybridization between the heterogeneous bivalent core nanoparticles (S1/2-II) and the monovalent satellite nanoparticles (S1'-I and S2'-I). Expanding on the demonstration, linear oligomer nanoassemblies (60 nm in diameter) with different lengths are also fabricated following DNA hybridization between the heterogeneous bivalent nanoparticles (S1/2-II) and their counterparts with complementary sequences (S1'/2'-II), as shown in Figure 2d.

2.3. Constructing Geometrically and Compositionally Diversified Nanoassemblies

The versatility of the MDT strategy is also demonstrated by employing it to construct geometrically and compositionally diversified nanoassemblies. In this case, a given valence of DNA patch is fabricated on the silver cubic nanoparticles and geometrically irregular diamond nanoparticles. The symbols used in Figure 3 are consistent with those defined previously, except that the letters “C” and “D” are used in place of “S” to

represent cubic and diamond nanoparticles. As shown in Figure 3a, silver cubic dimers, trimers of two configurations, and tetramers can be created following DNA hybridization among monovalent (C1-I and C1'-I), between bivalent (C1-II) and monovalent (C1'-I), and between trivalent (C1-III) and monovalent (C1'-I) silver nanocubes (50 nm of edge length), respectively. Likewise, nanocube-based linear oligomer nanoassemblies (50 nm of edge length) with different lengths can be readily fabricated through DNA hybridization of heterogeneous bivalent silver nanocubes (C1/2-II) and their counterparts with complementary sequences (C1'/2'-II), as shown in Figure 3b.

To demonstrate the construction of compositionally heterogeneous nanoassemblies using geometrically irregular nanoparticles, monovalence and divalence are first, respectively, fabricated on diamond nanoparticles with varying sizes. By reacting monovalent diamond (mean diameter: 10 nm) with monovalent silver cubes (100 nm of edge length) with complementary DNA patches, heterogeneous silver nanocube-diamond dimers are formed, as shown in Figure 3c. The reaction between bivalent diamond (mean diameters: 10 and 40 nm) and monovalent silver cubes (100 nm of edge length) further leads to the formation of silver cubic dimers with the diamond sandwiched in between, as shown in Figure 3c.

It is worth noting that the intense electromagnetic fields confined at the gap of silver cubic dimers can dramatically modify the photophysical properties of the sandwiched quantum emitter.^{21,35} Yet, precisely positioning a solid quantum emitter with irregular shape and tunable size, e.g., a diamond nanoparticle, in a nanogap remains highly challenging. Our success in creating the silver cubic dimers with a diamond nanoparticle sandwiched in between, as shown in

Figure 3c, demonstrates the strong capability of the MDT strategy for developing a wide variety of desired nano-architecture with nanometer precision.

2.4. Silver Cubic Dimer-Enhanced Spontaneous Emission of a Quantum Emitter

To demonstrate the conferred superior optical properties of nanoassemblies created by the MDT strategy, we investigate the modification of the spontaneous emission of a single diamond nanoparticle precisely positioned at the gap of a silver cubic dimer. To that goal, the spontaneous emission of a single silver cubic dimer with a diamond nanoparticle sandwiched in between, as shown in Figure 3c, is measured by fluorescence lifetime imaging microscopy (FLIM). FLIM is implemented using an excitation wavelength of 532 nm with the fluorescence signals collected in the wavelength range of 650–720 nm. Representative images for the obtained fluorescence intensity and lifetime distributions of NV centers in the diamond nanoparticle are shown in Figure 4a, whereas the corresponding lifetime decay is shown in Figure 4b as compared to that of a bare diamond nanoparticle. The silver cubic dimer is found to enable approximately 16-fold enhancement of the fluorescence intensity and about a 20-fold increase of the spontaneous emission rate as compared to the bare diamond particles. The simultaneously amplified fluorescence intensity and accelerated spontaneous emission dynamics of NV centers in diamond not only highlight the distinct optical properties of the silver cubic dimer-modified nanodiamond but also underscore the vast promise of the MDT strategy in DNA-directed self-assembly with high precision unbound by the geometry, dimension, and composition of the constituent nanoparticles. The enhanced spontaneous emission intensity and dynamics of NV centers could augment both the sensitivity and temporal resolution of an NV center-based magnetometer for quantum biological sensing and imaging of a weak magnetic field,³⁶ radical pairs,^{37,38} and other paramagnetic species.^{39,40}

3. CONCLUSIONS

In summary, we have developed a magnetic bead-assisted DNA cluster transfer strategy to fabricate regioselective DNA patches on colloidal nanoparticles with high precision. The DNA patches endow colloidal nanoparticles with valence bond-equivalent surface functionalities and allow specific and directional recognition interaction through DNA hybridizations. Given the generalizability of the MDT strategy, we leverage it to add a given valence of DNA patches to colloidal nanoparticles of different shapes, dimensions, and compositions. The versatility of the MDT strategy is reflected in the numerous types of fabricated nanoassemblies, including gold spherical dimer, trimer, tetramer, pentamer, gold spherical and silver cubic linear oligomer nanoassemblies with different lengths, silver nanocube-diamond heterogeneous dimers, and silver cubic dimers with a diamond particle sandwiched at the gap. The vast promise of the MDT strategy is further evidenced by the simultaneously amplified fluorescence intensity and accelerated spontaneous emission dynamics of a diamond nanoparticle precisely positioned at the gap of the silver nanocubic dimer. We envision that the developed MDT strategy can be readily extended to create molecule-like and structurally sophisticated hierarchical nanoassemblies harboring distinct optical and photophysical properties with potential

applications in biological sensing, optical physics, and catalytic chemistry.

4. EXPERIMENTAL SECTION

4.1. Preparation of Dock DNA-Functionalized AuNPs

Prior to use, colloidal AuNPs with a mean diameter of 40, 60, and 80 nm were subjected to centrifugation to concentrate 10 times (40 nm AuNPs, 8000 rpm for 10 min; 60 nm AuNPs, 5500 rpm for 10 min; 80 nm AuNPs, 2800 rpm for 10 min). The disulfide bond in the thiol-modified oligonucleotides (dock DNA) was reduced to monothiol using TCEP (120 mM, 1 h). The oligonucleotides were purified using size exclusion columns (G-25, GE Healthcare) to get rid of the small molecules (TCEP). Further, 80 μ L of a concentrated colloidal solution of 80 nm AuNPs was mixed with freshly dissolved dock DNA (250 μ M) in a 1:50,000 ratio (1:10,000 for 40 nm AuNPs and 1:20,000 for 60 nm AuNPs) in distilled water, and the mixture was incubated for 2 h at room temperature (300 rpm). Then, 10 μ L of a phosphate-buffered solution (PBS) (100 mM, pH = 7.4) was added to the mixture. After 30 min, 1 μ L of a NaCl solution (2 M) was added every 20 min four times and then 2 μ L of a NaCl solution (2 M) every 30 min three times. The NaCl concentration was gradually increased by the salt-aging method to ensure the full coverage of AuNPs with dock DNA. The final concentration of NaCl was 200 mM, and the mixture was incubated at room temperature (300 rpm) overnight. The AuNP–DNA conjugates were purified by centrifugation. Before the first centrifugation, Tween 20 was added to the mixture to reduce the adsorption of AuNPs on the microcentrifuge tube wall. The concentration of Tween 20 in the AuNP–DNA conjugate solution was 0.1%. Freshly prepared, fully covered 40, 60, and 80 nm AuNPs did not precipitate in the PBS buffer (100 mM, pH = 8.0). This high-salt resistance property of fully covered AuNPs makes it possible to assemble a variety of colloidal metamaterials through DNA hybridization.

4.2. Preparation of Dock DNA-Functionalized Silver Nanocubes

Prior to use, the colloidal solutions, 50 and 100 nm silver nanocubes (1 mg/mL in ethanol, PVP coating, nanoComposix), were subjected to centrifugation (50 nm silver nanocubes: 5000 rpm for 10 min; 100 nm AuNPs: 2500 rpm for 10 min) to exchange to a water solution. The disulfide bond in the thiol-modified oligonucleotides (dock DNA) was reduced to monothiol using TCEP (20 mM, 1 h). The dock DNA was purified using size exclusion columns (G-25, GE Healthcare) to get rid of the small molecules (TCEP). Then, 50 μ L of water exchanged colloidal solution of 100 nm silver nanocubes was mixed with 50 μ L of freshly dissolved dock DNA in a 1:100,000 (particle molar/molecule molar) ratio (1:10,000 for 50 nm silver nanocubes) in water, and the mixture was incubated for 36 h at room temperature (300 rpm). Then, 100 μ L of PBS buffer (150 mM, pH = 7.4) was added to the mixture. After 12 h, 100 μ L of PBS buffer was added. The NaCl concentration was gradually increased by the salt-aging method to ensure the full coverage of silver nanocubes with dock DNA. The final concentration of NaCl was 100 mM, and the mixture was incubated at room temperature (300 rpm) overnight. The silver nanocube–DNA conjugates were purified by centrifugation three times (0.1% Tween 20 was added to the solution to reduce the adsorption of silver nanocube–DNA conjugates on the microcentrifuge tube wall).

4.3. Preparation of Dock DNA-Functionalized Nanodiamonds

Prior to use, the colloidal solutions of 10 and 40 nm biotin-modified nanodiamonds (1 mg/mL, Adámas Nanotechnologies) were mixed with freshly dissolved neutravidin (10 mg/mL) in a 1:100 v/v ratio (1:10 for 40 nm nanodiamond) in water, and the mixture was incubated for 2 h at room temperature (300 rpm). The nanodiamond–avidin conjugates were purified by centrifugation (40 nm nanodiamond: 5000 rpm for 10 min, 10 nm nanodiamond: 8000 rpm for 10 min) three times to remove excess neutravidin. Then, the

nanodiamond–avidin conjugates were mixed with dock DNA (biotin-labeled DNA (100 μM)) for 2 h at room temperature (300 rpm). The nanodiamond–DNA conjugates were purified by centrifugation (40 nm nanodiamond: 5000 rpm for 10 min, 10 nm nanodiamond: 8000 rpm for 10 min) three times to remove excess dock DNA.

4.4. Preparation of DNA-Coated Magnetic Beads

Prior to use, 100 μL of fresh hydrophilic streptavidin-conjugated magnetic beads (4 mg/mL, New England Biolabs) was subjected to purification three times using a magnet to attract streptavidin magnetic beads to one side of the microcentrifuge tube and replacing the medium with 1 \times Tris–acetate–EDTA buffer (TAE buffer). The purpose of purification is to get rid of sodium azide in the fresh hydrophilic streptavidin magnetic bead suspension. The purified streptavidin-conjugated magnetic beads were mixed with 32 μL of biotin-labeled DNA (coating DNA (200 nM)), and the mixture was incubated for 30 min in a rotator at 10 rpm at room temperature. The DNA-coated streptavidin-conjugated magnetic beads were subjected to purification three times by the same magnet-attracting and medium-replacing method mentioned above.

4.5. Magnetic Bead-Based DNA Cluster Transferring (MDT)

The purified DNA-coated magnetic beads were mixed with 32 μL of patch-hold DNA (220 nM), and the mixture was incubated for 1 h in a rotator at 10 rpm at room temperature. The purpose of the concentration of patch-hold DNA being 10% higher than the concentration of biotin-labeled DNA is to let free patch-hold DNA fully hybridize with biotin-labeled DNA coated on the surface of magnetic beads. The conjugate of DNA-coated magnetic beads and patch-hold DNA was subjected to purification three times by the same magnet-attracting and medium-replacing method mentioned above. Then, the purified conjugate of a magnetic bead, biotin-labeled DNA, and patch-hold DNA was mixed with 32 μL of patch DNA (250 nM), and the mixture was incubated for 1 h in a rotator at 10 rpm at room temperature. The conjugate of a DNA-coated magnetic bead, patch-hold DNA, and patch DNA was subjected to purification three times by the same magnet-attracting and medium-replacing method mentioned above.

Then, the dock DNA-functionalized AuNP solution was mixed with the purified conjugate of a magnetic bead, biotin-labeled DNA, patch-hold DNA, and patch DNA. The mixture was incubated for 5 h in a rotator at 10 rpm at room temperature. Then, the conjugation of the DNA-coated magnetic bead, patch-hold DNA, patch DNA, and dock DNA-functionalized AuNPs was subjected to purification three times.

Then, 320 μL of transfer DNA (250 nM) was mixed with the purified conjugation of a magnetic bead, biotin-labeled DNA, patch-hold DNA, patch DNA, and dock DNA-functionalized AuNPs. The mixture was incubated for 16 h in a rotator at 10 rpm at room temperature. The purpose of using excessive transfer DNA is to increase the amount of DNA-patched AuNPs.

4.6. Self-Assembly of Colloidal Molecules

The absorbance of a DNA-patched AuNP solution was measured by a UV–vis spectrophotometer (PerkinElmer). The concentration of DNA-patched AuNPs was calculated based on the Beer–Lambert law. Based on the concentration of DNA-patched AuNPs, DNA-patched AuNPs with complementary DNA patch sequences were mixed in a certain volume-to-volume ratio, and the mixture was incubated for 15 min at room temperature.

4.7. Scanning Electron Microscopy (SEM) Imaging

For SEM imaging, 10 μL of a sample solution was deposited on a plasma-treated silicon wafer for 10 min, after which excess solution was wicked away with filter paper and dried by nitrogen gas. Imaging was performed using a Tescan Mira 3 GM SEM operated at an acceleration voltage of 5 kV.

4.8. Statistical Analysis of the Yield of Various Gold Spherical Nanoassemblies

Statistical analysis was performed on SEM images by counting the number of different types of nanoassemblies to calculate the yield of

homogeneous nanoclusters of 40, 60, and 80 nm gold nanoparticles with monovalent (I), divalent (II), trivalent (III), and tetravalent (IV), respectively. The number of SEM images used and the number of nanoclusters analyzed are summarized in Tables S2 and S3.

4.9. FLIM Imaging

A customized confocal microscope (based on ISS Q2 laser scanning nanoscope) with single-molecule detection sensitivity was used for single-particle intensity and fluorescence lifetime imaging. The excitation source was a Fianium supercontinuum SC-400 laser (6 ps pulse width and A 42 MHz repetition rate) equipped with an NKT acousto-optic tunable filter (AOTF) to select a specific wavelength. The incident wavelength of 532 nm was used for exciting the colloidal metamaterials. The excitation light, further cleaned up by a laser-line band-pass filter (532/10), was reflected by a dichroic mirror and focused onto the sample on an inverted microscope (Olympus, IX70). A water immersion objective (Olympus 60 \times , 1.2 numerical aperture (NA)) was used for focusing the laser light onto the sample and for collecting the fluorescence intensity emission from the sample. The fluorescence signal that passed through the dichroic mirror and a band-pass filter (650–720 nm, Chroma) was focused through a 75 μm pinhole to a single-photon avalanche photodiode (SPAD) (SPCM-AQRH-14, Excelitas Technologies) detector. The imaging in our setup was performed with Galvo-controlled mirrors with related electronics and optics controlled through the 3X-DAC control card. The software module in ISS VistaVision for data acquisition and data processing along with this time-correlated single-photon counting (TCSPC) module from Becker & Hickl (SPC-150) facilitate fluorescence lifetime measurements. The fluorescence intensity decays were analyzed in terms of an exponential model. The values of fluorescence lifetimes were determined using VistaVision software with nonlinear least-squares fitting. Fluorescence lifetimes were estimated by fitting to a χ^2 value of less than 1.2 and a residual trace that was symmetrical about the zero axis. All analyses were performed using VistaVision software and Originlab.

■ ASSOCIATED CONTENT

Supporting Information

The Supporting Information is available free of charge at <https://pubs.acs.org/doi/10.1021/jacsau.3c00013>.

Materials and chemicals; DNA sequences; SEM images of the dimer, trimer, tetramer, and pentamer: (1) 40 nm AuNPs, (2) 60 nm AuNPs as the core and 40 nm AuNPs as the satellite nanoparticles, (3) 80 nm AuNPs as the core and 40 nm AuNPs as the satellite nanoparticles, (4) 80 nm AuNPs as the core and 60 nm AuNPs as the satellite nanoparticles, and (5) 80 nm AuNPs; off-axis angle analysis for silver cubic dimers; dark-field spectra for (a) gold dimer, (b) gold trimer, (c) gold tetramer, and (d) gold pentamer; yields of homogeneous nanoclusters; number of SEM images analyzed for the statistical yield; and number of nanoclusters analyzed for the statistical yield (PDF)

■ AUTHOR INFORMATION

Corresponding Author

Ishan Barman – Department of Mechanical Engineering, Johns Hopkins University, Baltimore, Maryland 21218, United States; Department of Oncology and Department of Radiology & Radiological Science, Johns Hopkins University School of Medicine, Baltimore, Maryland 21287, United States; orcid.org/0000-0003-0800-0825; Email: ibarman@jhu.edu

Authors

Le Liang – *The Institute for Advanced Studies, Wuhan University, Wuhan 430072, China; Department of Mechanical Engineering, Johns Hopkins University, Baltimore, Maryland 21218, United States*

Lintong Wu – *Department of Mechanical Engineering, Johns Hopkins University, Baltimore, Maryland 21218, United States*

Peng Zheng – *Department of Mechanical Engineering, Johns Hopkins University, Baltimore, Maryland 21218, United States; orcid.org/0000-0001-5907-8505*

Tao Ding – *The Institute for Advanced Studies, Wuhan University, Wuhan 430072, China*

Krishanu Ray – *Division of Vaccine Research, Institute of Human Virology, Department of Biochemistry and Molecular Biology, University of Maryland School of Medicine, Baltimore, Maryland 21201, United States*

Complete contact information is available at:
<https://pubs.acs.org/10.1021/jacsau.3c00013>

Author Contributions

[#]L.L., L.W., and P.Z. contributed equally to this work. The manuscript was written through contributions of all authors. All authors have given approval to the final version of the manuscript.

Author Contributions

CRedit: **Le Liang** conceptualization, data curation, formal analysis, investigation, methodology, validation, writing-original draft, writing-review & editing; **Lintong Wu** data curation, formal analysis, investigation, methodology, validation, writing-original draft, writing-review & editing; **Peng Zheng** formal analysis, investigation, methodology, validation, writing-original draft, writing-review & editing; **Tao Ding** data curation; **Krishanu Ray** data curation, investigation, methodology; **Ishan Barman** conceptualization, data curation, formal analysis, funding acquisition, investigation, methodology, project administration, resources, supervision, writing-original draft, writing-review & editing.

Notes

The authors declare no competing financial interest.

ACKNOWLEDGMENTS

This research was supported by start-up funding from Wuhan University, the National Institute of Biomedical Imaging and Bioengineering (P41-EB015871), the National Institute of General Medical Sciences (DP2GM128198), and the National Institute of Allergy and Infectious Diseases (R56-AI172487).

REFERENCES

- (1) Boles, M. A.; Engel, M.; Talapin, D. V. Self-Assembly of Colloidal Nanocrystals: From Intricate Structures to Functional Materials. *Chem. Rev.* **2016**, *116*, 11220–11289.
- (2) Hsu, S.-W.; Rodarte, A. L.; Som, M.; Arya, G.; Tao, A. R. Colloidal Plasmonic Nanocomposites: From Fabrication to Optical Function. *Chem. Rev.* **2018**, *118*, 3100–3120.
- (3) Hueckel, T.; Hocky, G. M.; Sacanna, S. Total synthesis of colloidal matter. *Nat. Rev. Mater.* **2021**, *6*, 1053–1069.
- (4) Liang, L.; Zheng, P.; Jia, S.; Ray, K.; Chen, Y.; Barman, I. DNA Self-Assembled Plasmonic Nanodiamonds for Biological Sensing *bioRxiv* 2021 DOI: [10.1101/2021.11.09.467982](https://doi.org/10.1101/2021.11.09.467982).
- (5) Sun, Y.; Terrones, M.; Schaak, R. E. Colloidal Nanostructures of Transition-Metal Dichalcogenides. *Acc. Chem. Res.* **2021**, *54*, 1517–1527.
- (6) Yin, Y.; Talapin, D. The chemistry of functional nanomaterials. *Chem. Soc. Rev.* **2013**, *42*, 2484–2487.
- (7) Dreaden, E. C.; Alkilany, A. M.; Huang, X.; Murphy, C. J.; El-Sayed, M. A. The golden age: gold nanoparticles for biomedicine. *Chem. Soc. Rev.* **2012**, *41*, 2740–2779.
- (8) Yang, X.; Yang, M.; Pang, B.; Vara, M.; Xia, Y. Gold Nanomaterials at Work in Biomedicine. *Chem. Rev.* **2015**, *115*, 10410–10488.
- (9) Choueiri, R. M.; Galati, E.; Thérien-Aubin, H.; Klinkova, A.; Larin, E. M.; Querejeta-Fernández, A.; Han, L.; Xin, H. L.; Gang, O.; Zhulina, E. B.; Rubinstein, M.; Kumacheva, E. Surface patterning of nanoparticles with polymer patches. *Nature* **2016**, *538*, 79–83.
- (10) Gong, Z.; Hueckel, T.; Yi, G.-R.; Sacanna, S. Patchy particles made by colloidal fusion. *Nature* **2017**, *550*, 234–238.
- (11) Qiu, H.; Gao, Y.; Boott, C. E.; Gould, O. E. C.; Harniman, R. L.; Miles, M. J.; Webb, S. E. D.; Winnik, M. A.; Manners, I. Uniform patchy and hollow rectangular platelet micelles from crystallizable polymer blends. *Science* **2016**, *352*, 697–701.
- (12) He, M.; Gales, J. P.; Ducrot, É.; Gong, Z.; Yi, G.-R.; Sacanna, S.; Pine, D. J. Colloidal diamond. *Nature* **2020**, *585*, 524–529.
- (13) Nykypanchuk, D.; Maye, M. M.; van der Lelie, D.; Gang, O. DNA-guided crystallization of colloidal nanoparticles. *Nature* **2008**, *451*, 549–552.
- (14) Costi, R.; Saunders, A. E.; Banin, U. Colloidal Hybrid Nanostructures: A New Type of Functional Materials. *Angew. Chem., Int. Ed.* **2010**, *49*, 4878–4897.
- (15) Li, Z.; Fan, Q.; Yin, Y. Colloidal Self-Assembly Approaches to Smart Nanostructured Materials. *Chem. Rev.* **2022**, *122*, 4976–5067.
- (16) Samanta, D.; Zhou, W.; Ebrahimi, S. B.; Petrosko, S. H.; Mirkin, C. A. Programmable Matter: The Nanoparticle Atom and DNA Bond. *Adv. Mater.* **2022**, *34*, No. 2107875.
- (17) Fan, J. A.; Wu, C.; Bao, K.; Bao, J.; Bardhan, R.; Halas, N. J.; Manoharan, V. N.; Nordlander, P.; Shvets, G.; Capasso, F. Self-Assembled Plasmonic Nanoparticle Clusters. *Science* **2010**, *328*, 1135–1138.
- (18) Tanwar, S.; Haldar, K. K.; Sen, T. DNA Origami Directed Au Nanostar Dimers for Single-Molecule Surface-Enhanced Raman Scattering. *J. Am. Chem. Soc.* **2017**, *139*, 17639–17648.
- (19) Fang, W.; Jia, S.; Chao, J.; Wang, L.; Duan, X.; Liu, H.; Li, Q.; Zuo, X.; Wang, L.; Wang, L.; Liu, N.; Fan, C. Quantizing single-molecule surface-enhanced Raman scattering with DNA origami metamolecules. *Sci. Adv.* **2019**, *5*, No. eaau4506.
- (20) Liang, L.; Zheng, P.; Zhang, C.; Barman, I. A Programmable DNA-Silicification-Based Nanocavity for Single-Molecule Plasmonic Sensing. *Adv. Mater.* **2021**, *33*, No. 2005133.
- (21) Acuna, G. P.; Möller, F. M.; Holzmeister, P.; Beater, S.; Lalkens, B.; Tinnefeld, P. Fluorescence Enhancement at Docking Sites of DNA-Directed Self-Assembled Nanoantennas. *Science* **2012**, *338*, 506–510.
- (22) Jin, R.; Pei, Y.; Tsukuda, T. Controlling Nanoparticles with Atomic Precision. *Acc. Chem. Res.* **2019**, *52*, No. 1.
- (23) Gwo, S.; Chen, H.-Y.; Lin, M.-H.; Sun, L.; Li, X. Nano-manipulation and controlled self-assembly of metal nanoparticles and nanocrystals for plasmonics. *Chem. Soc. Rev.* **2016**, *45*, 5672–5716.
- (24) Kaur, V.; Tanwar, S.; Kaur, G.; Sen, T. DNA-Origami-Based Assembly of Au@Ag Nanostar Dimer Nanoantennas for Label-Free Sensing of Pyocyanin. *ChemPhysChem* **2021**, *22*, 160–167.
- (25) Tanwar, S.; Kaur, V.; Kaur, G.; Sen, T. Broadband SERS Enhancement by DNA Origami Assembled Bimetallic Nanoantennas with Label-Free Single Protein Sensing. *J. Phys. Chem. Lett.* **2021**, *12*, 8141–8150.
- (26) Yi, C.; Liu, H.; Zhang, S.; Yang, Y.; Zhang, Y.; Lu, Z.; Kumacheva, E.; Nie, Z. Self-limiting directional nanoparticle bonding governed by reaction stoichiometry. *Science* **2020**, *369*, 1369–1374.

(27) Wang, Y.; Wang, Y.; Breed, D. R.; Manoharan, V. N.; Feng, L.; Hollingsworth, A. D.; Weck, M.; Pine, D. J. Colloids with valence and specific directional bonding. *Nature* **2012**, *491*, 51–55.

(28) Yao, G.; Li, J.; Li, Q.; Chen, X.; Liu, X.; Wang, F.; Qu, Z.; Ge, Z.; Narayanan, R. P.; Williams, D.; Pei, H.; Zuo, X.; Wang, L.; Yan, H.; Feringa, B. L.; Fan, C. Programming nanoparticle valence bonds with single-stranded DNA encoders. *Nat. Mater.* **2020**, *19*, 781–788.

(29) Chen, G.; Gibson, K. J.; Liu, D.; Rees, H. C.; Lee, J.-H.; Xia, W.; Lin, R.; Xin, H. L.; Gang, O.; Weizmann, Y. Regioselective surface encoding of nanoparticles for programmable self-assembly. *Nat. Mater.* **2019**, *18*, 169–174.

(30) Sun, S.; Yang, S.; Xin, H. L.; Nykypanchuk, D.; Liu, M.; Zhang, H.; Gang, O. Valence-programmable nanoparticle architectures. *Nat. Commun.* **2020**, *11*, No. 2279.

(31) Trinh, T.; Liao, C.; Toader, V.; Barlóg, M.; Bazzi, H. S.; Li, J.; Sleiman, H. F. DNA-imprinted polymer nanoparticles with mono-dispersity and prescribed DNA-strand patterns. *Nat. Chem.* **2018**, *10*, 184–192.

(32) Edwardson, T. G. W.; Lau, K. L.; Bousmail, D.; Serpell, C. J.; Sleiman, H. F. Transfer of molecular recognition information from DNA nanostructures to gold nanoparticles. *Nat. Chem.* **2016**, *8*, 162–170.

(33) Zhang, Y.; Chao, J.; Liu, H.; Wang, F.; Su, S.; Liu, B.; Zhang, L.; Shi, J.; Wang, L.; Huang, W.; Wang, L.; Fan, C. Transfer of Two-Dimensional Oligonucleotide Patterns onto Stereocontrolled Plasmonic Nanostructures through DNA-Origami-Based Nanoimprinting Lithography. *Angew. Chem., Int. Ed.* **2016**, *55*, 8036–8040.

(34) Ding, B.; Deng, Z.; Yan, H.; Cabrini, S.; Zuckermann, R. N.; Bokor, J. Gold Nanoparticle Self-Similar Chain Structure Organized by DNA Origami. *J. Am. Chem. Soc.* **2010**, *132*, 3248–3249.

(35) Gao, B.; Arya, G.; Tao, A. R. Self-orienting nanocubes for the assembly of plasmonic nanojunctions. *Nat. Nanotechnol.* **2012**, *7*, 433–437.

(36) Vershovskii, A. K.; Dmitriev, A. K. A Weak Magnetic Field Sensor Based on Nitrogen-Vacancy Color Centers in a Diamond Crystal. *Tech. Phys.* **2020**, *65*, 1301–1306.

(37) Liu, H.; Plenio, M. B.; Cai, J. Scheme for Detection of Single-Molecule Radical Pair Reaction Using Spin in Diamond. *Phys. Rev. Lett.* **2017**, *118*, No. 200402.

(38) Mzyk, A.; Sigaeva, A.; Schirhagl, R. Relaxometry with Nitrogen Vacancy (NV) Centers in Diamond. *Acc. Chem. Res.* **2022**, *55*, 3572–3580.

(39) Barton, J.; Gulka, M.; Tarabek, J.; Mindarava, Y.; Wang, Z.; Schimer, J.; Raabova, H.; Bednar, J.; Plenio, M. B.; Jelezko, F.; Nesladek, M.; Cigler, P. Nanoscale Dynamic Readout of a Chemical Redox Process Using Radicals Coupled with Nitrogen-Vacancy Centers in Nanodiamonds. *ACS Nano* **2020**, *14*, 12938–12950.

(40) Li, C.; Chen, M.; Lyzwa, D.; Cappellaro, P. All-Optical Quantum Sensing of Rotational Brownian Motion of Magnetic Molecules. *Nano Lett.* **2019**, *19*, 7342–7348.